Earth-Abundant Mixed-Metal Catalysts for Hydrocarbon Oxygenation

Earth-abundant mixed-metal catalysts for hydrocarbon oxygenation

James R. Pankhurst,[a] Massimiliano Curcio,[a] Stephen Sproules,*[b] Guy C. Lloyd-Jones,*[a] and Jason B. Love*[a]

[a] EaStCHEM School of Chemistry, The University of Edinburgh, Joseph Black Building, David Brewster Road, Edinburgh, EH9 3FJ, UK. E-mail: jason.love@ed.ac.uk; guy.lloyd-jones@ed.ac.uk; stephen.sproules@glasgow.ac.uk.

[b] WestCHEM School of Chemistry, University of Glasgow, Glasgow, G12 8QQ, UK.

ABSTRACT: The oxygenation of aliphatic and aromatic hydrocarbons using earth-abundant iron and copper catalysts and 'green' oxidants such as hydrogen peroxide is becoming increasingly important to atom-economical chemical processing. In light of this, we describe that dinuclear Cu^{II} complexes of pyrrolic Schiff-base macrocycles, in combination with $FeCl_3$, catalyze the oxygenation of π-activated benzylic substrates with hydroperoxide oxidants at room temperature and low loadings, representing a novel design in oxidation catalysis. Mass spectrometry and EXAFS analysis indicate that a cooperative action between Cu^{II} and Fe^{III} occurs, most likely due to the interaction of $FeCl_3$ or $FeCl_4^-$ with the dinuclear Cu^{II} macrocycle. Voltammetric measurements highlight a modulation of both Cu^{II} and Fe^{III} redox potentials in this adduct, but EPR spectroscopy indicates that any Cu-Fe intermetallic interaction is weak. High ketone/alcohol product ratios, a small reaction constant (Hammett analysis) and small KIE for H-atom abstraction point towards a free-radical reaction. However, lack of reactivity with cyclohexane, oxidation of 9,10-dihydroanthracene, oxygenation by the hydroperoxide MPPH (radical mechanistic probe), and oxygenation in N_2-purge experiments indicate a metal-based reaction. Through detailed reaction monitoring and associated kinetic modelling, a network of oxidation pathways is proposed that includes "well-disguised" radical chemistry via the formation of metal-associated radical intermediates.

Introduction

The combination of earth-abundant metals such as Fe or Cu, with oxidants such as O_2 or H_2O_2 offers "green" alternatives to more traditional, toxic, stoichiometric or catalytic chromium and manganese reagents for the oxygenation of alkanes. The process has a strong foundation in understanding enzymatic oxygenation of hydrocarbons.[1-7] Cytochrome P450 and peroxidase enzymes react aerobically through high-oxidation-state iron oxo (Fe^{IV}=O, "ferryl heme") complexes.[8-10] Tyrosinase enzymes feature bimetallic Cu^I active sites that oxidize catechol to *ortho*-quinone.[11-12] Methane monooxygenase (MMO) enzymes contain either copper or iron[13-14] and oxidize the strong C–H bonds of methane (H_{Diss} = 439 kJ mol^{-1}).[15-16] This has led to the development of oxygenation catalysts based on copper and iron complexes[17] that incorporate the M(μ-O_2)M diamond motif,[18-21] reactive iron-oxo and -peroxo porphyrins,[22-27] and non-heme Fe^{IV}=O[28-32] or Fe^V=O[33] functionalities.

Simple transition metal salts of copper and iron have also been used in non-biomimetic approaches to oxygenation catalysis, mainly in combination with hydrogen peroxide (H_2O_2) or *tert*-butyl hydroperoxide (*t*BuOOH, TBHP) as the oxidant. The reaction between CuBr and TBHP forms mixtures of *t*BuO$^\bullet$ (alkoxyl) and *t*BuOO$^\bullet$ (peroxyl) radicals that carry out hydrogen-atom abstraction (HAA) from hydrocarbons.[34] $CuCl_2$, CuCl and copper metal catalyze oxygenation of π-activated benzylic substrates using TBHP.[35-36] Furthermore, copper acetate catalyzes the oxidation of aromatic C–H bonds using O_2 as an oxidant.[37] The related Kharasch-Sosnovsky reaction of dialkyl-peroxides leads to etherification of hydrocarbon substrates and is typically catalyzed by Cu^I salts,[38-41] and coordination complexes of Cu^I have also been implemented in radical reactions.[42] Simple iron salts (most commonly $FeCl_3$) and their complexes catalyze oxygenation reactions of hydrocarbon substrates with high bond-dissociation energies (BDEs), including cyclohexane.[43-56] The bulk of these reactions are described by Fenton mechanisms,[57-58] in which the role of iron is to generate highly reactive hydroxyl,[59] *tert*-butoxyl[60] and *tert*-butyl peroxyl[61] free radicals from the hydroperoxide.

Mixtures of metal compounds can act as *tandem* catalysts for oxygenation reactions.[62-65] Combinations of Fe^{II} and Cr^{II} diketonates carry out tandem oxygenation and epoxidation catalysis of cyclohexene.[66-67] Additionally, copper acetate and $FeCl_3$ mixtures act as catalysts for a complex series of C–C and C–O bond forming reactions, although these reactions require high catalyst loadings.[68] A mixture of Fe_2SO_4 and $CuCl_2$ catalyzes oxidation and isomerization of alkene-containing organoperoxides, yielding ketone products, with the postulated mechanism showing the two metal ions participating in tandem.[69] In terms of *cooperative* catalysis, mixtures of copper and iron (in the form of salts, complexes or nanoparticles) have been used to successfully promote cross-coupling reactions,[70] including those that form new C–C bonds,[71-74] C–O bonds,[75-76] C–S bonds,[77] and also *N*-arylation.[78-80] In contrast, there is surprisingly little use of mixtures of metals and their complexes in cooperative catalysis for the direct functionalization of hydrocarbon C–H bonds. In one example, amination of an allylic C–H bond was achieved by a palladium acetate catalyst, but only when a Cr^{III} catalyst was also present to aminate the palladium-allyl intermediate.[81]

Based on these precedents we sought to employ dinuclear Cu^{II} complexes of Schiff-base pyrrole macrocycles as catalysts for hydrocarbon oxygenation (Figure 1).[82-83] Through variation of various components in these macrocycles, important parameters such as inter-nuclear separation and cavity size can be controlled.[84-85] The macrocyclic clefts offered by these complexes are reminiscent of supramolecular flasks, where catalytic and stoichiometric reactions that are disfavored in the bulk phase,

can take place within the host structure due to the increased effective concentration and lowered entropy.[86-89] Dinuclear Fe^{II} Pacman diporphyrin complexes activate O_2, leading to reactive Fe^{IV}=O complexes (through photolysis) that oxidize hydrocarbon substrates to generate alcohols.[22] We anticipated that reactions between complexes **A**, **B**, or **C** (Figure 1) and hydroperoxides might form reactive species akin to diamond MO_2M complexes,[21,90-91] as the structurally related Schiff-base Pacman complexes of Co^{II} catalyze the microscopic reverse dioxygen-reduction reaction.[92-94] Electrochemical measurements have indicated that the Cu^{III} oxidation state is also accessible for these complexes, leading to the possibility of the formation of Cu^{III}–OH complexes which could take place in HAA reactions.[95-98]

We report here the use of dinuclear Cu^{II} complexes for the catalytic oxygenation of π-activated, benzylic hydrocarbon substrates, using hydroperoxide oxidants. We find that the activity, stability, and operating temperature of the catalyst improves substantially by the addition of $FeCl_3$, and we report the attempted characterization of the catalytically active species through detailed spectroscopic and voltammetric methods, as well as the elucidation of a plausible reaction network through kinetics studies. To the best of our knowledge, there are no previous reports of mixtures of copper and iron compounds being used to catalyze the oxygenation of hydrocarbon bonds.

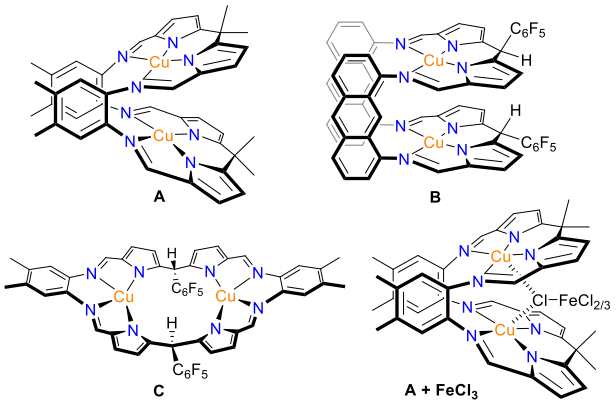

Figure 1. Dinuclear Cu^{II} macrocycles used as pre-catalysts for benzylic hydrocarbon oxygenation and the proposed pre-catalyst arising from **A** + $FeCl_3$. Complexes **A** and **B** adopt Pacman configurations and feature different spacer groups (Cu···Cu = 3.695 / 3.738 Å for **A** and 4.818(3) Å for **B**). Complex **C** adopts a bowl geometry (Cu···Cu = 6.493(6) Å).

Results and Discussion

Catalysis with bimetallic Cu^{II} macrocycles

Initial oxygenation reactions using the bimetallic Cu^{II} complexes **A** – **C** (0.2 mol%) were carried out in d_3-MeCN, using TBHP as the oxidant (Scheme 1). Xanthene was chosen as the substrate due to the low bond-dissociation energy (BDE) of its benzylic C–H bond (H_{Diss} = 75.5 kcal mol^{-1}).[99] All three complexes are catalytically inactive at room temperature, but on heating at 333 K the substrate is consumed, as evidenced by the loss of the benzylic proton resonance at 4.05 ppm in the ^{1}H NMR spectrum.

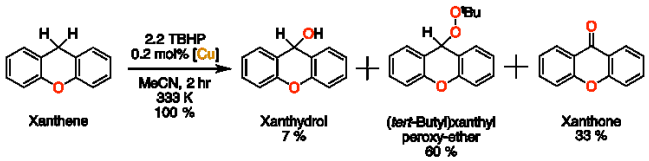

Scheme 1. Oxygenation of xanthene catalyzed by the dinuclear Cu^{II} complexes **A** – **C** at 333 K (yields determined by ^{1}H NMR spectroscopy).

The three products formed were identified by NMR/MS as the benzylic alcohol (xanthydrol, **ROH**), the organo-peroxide ((*tert*-butyl)xanthyl peroxy-ether, **ROOtBu**) and the benzylic ketone (xanthone, **RO**) after isolating the products on a preparative scale. One co-product of the reaction is *tert*-butanol, identified by the singlet resonance at 1.17 ppm of the methyl protons. Importantly, no 9,9'-bixanthene is seen, a homo-coupling product which might be expected to form if an organic free-radical reaction mechanism operates through HAA from xanthene.[100]

The concentration profiles for xanthene and its three oxygenated products were determined by ^{1}H NMR spectroscopy (Figure 2) with 93% conversion of the substrate seen within 30 min, giving a formal initial turnover frequency (TOF) of 930 h^{-1}.

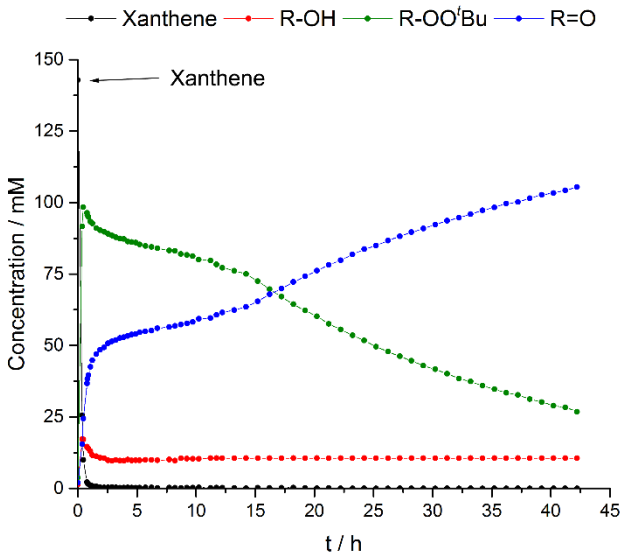

Figure 2. Monitoring the oxygenation of xanthene by 2.2 eq. TBHP, catalyzed by 0.2 mol% of complex **C** at 333 K in d_3-MeCN (concentrations determined by ^{1}H NMR integration). Interpolation between the data-points is provided solely as an aid to the eye.

After 2 h, the oxidation products **ROOtBu** and **RO** are formed in yields of 60% and 33%, respectively, with **ROH** in 7% yield. After this period, the concentrations of both **ROOtBu** and **RO** almost plateau for 10 h before the peroxy-ether slowly converts to the ketone through auto-oxidation at an approximate initial rate of 2×10^{-7} mol dm^{-3} s^{-1}. At room temperature, the background (non-catalyzed) oxidation of isolated **ROOtBu** is found to be slow (1×10^{-8} mol $dm^{-3}s^{-1}$) but is accelerated in the presence of 0.2 mol% of **C** (2×10^{-6} mol dm^{-3} s^{-1}). The slow oxidation of ROOtBu during the first 10 hours (Figure 2) suggests that the active catalyst inhibits the auto-oxidation during this stage.

Variation of the ligand scaffold in the macrocyclic complexes **A** – **C** causes dramatic changes in terms of their geometric and electronic properties, evident from their solid-state structures and electrochemical behaviour.[82-83] Despite these differences, varying the catalyst **A** – **C** did not change the activity or distribution of products, nor did it make the catalyst more or less susceptible to deactivation or inhibition. As the dipyrromethane groups containing *meso*-H substituents in complexes **B** and **C** could potentially undergo oxidation chemistry to dipyrrins,[101-102] only complex **A** was used to study the catalytic reactions in detail.

Mixed-metal catalysis

Whilst the Cu^{II} complexes are highly active xanthene oxygenation catalysts, this activity quickly arrests. In order to address this issue, $FeCl_3$ was employed initially as a simple Fe^{III} co-catalyst, as it has been demonstrated previously to catalyze the oxidation of benzylic alcohol substrates.[46] We hypothesized that this mixed-metal system would carry out *tandem* catalysis, with the Cu^{II} complex catalyzing xanthene oxygenation to form a mixture of **ROH** and **ROOtBu** and $FeCl_3$ catalyzing the formation of **RO** in improved yields with shorter reaction times.

Surprisingly, at catalyst loadings of 0.1 mol% **A** and 0.1 mol% $FeCl_3$, the reaction proceeds at room temperature; **A** shows negligible activity at room temperature, and $FeCl_3$ achieves only 13% conversion after 2 h, whereas the **A**/$FeCl_3$ mixture achieves 80% conversion within 2 h. Reaction monitoring by ^{1}H NMR spectroscopy revealed that the substrate is consumed after 4 h (Scheme 2, Figure 3), forming 72% **ROOtBu**, 19% **RO** and 9% **ROH**. Longer reaction times (12 h) and higher relative concentrations of TBHP are found to drive the selectivity towards the ketone product (in excess of 80%, Figure 3). It is significant that the addition of $FeCl_3$ both limits deactivation of the Cu^{II} catalyst and enhances reaction rate, implying that *cooperative* catalysis is taking place.

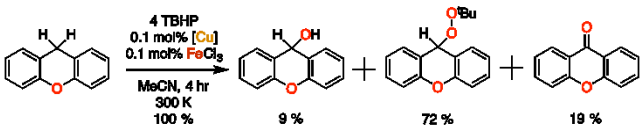

Scheme 2. Xanthene oxygenation catalyzed by a mixture of $FeCl_3$ and **A**, at 300 K (yields after 4 h shown, determined by ^{1}H NMR spectroscopy).

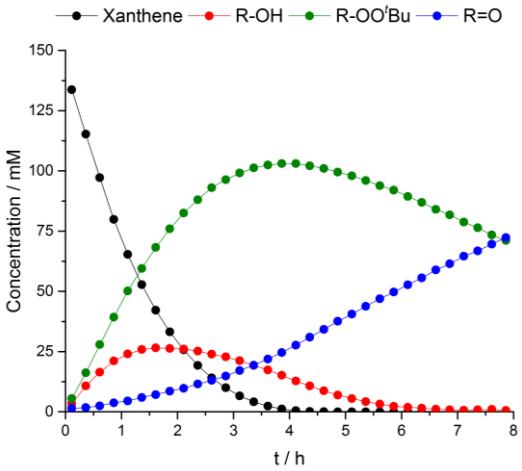

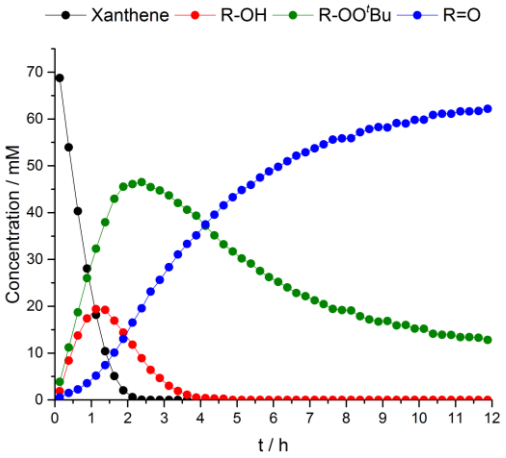

Figure 3. Monitoring xanthene oxygenation by TBHP catalyzed by mixtures of **A** and $FeCl_3$ at 300 K in d_3-MeCN (concentrations determined by ^{1}H NMR spectroscopy). Top: $[xanthene]_0$ = 150 mM, $[TBHP]_0$ = 575 mM, $[\mathbf{A}]_0$ = 150 μM, $[FeCl_3]_0$ = 150 μM. Bottom: $[xanthene]_0$ = 75 mM, $[TBHP]_0$ = 300 mM, $[\mathbf{A}]_0$ = 150 μM, $[FeCl_3]_0$ = 150 μM. Interpolation between the data-points is provided solely as an aid to the eye.

To test the stability of the catalyst further, recycling was attempted. The reaction between xanthene and 4 eq. of TBHP at room temperature, catalyzed by 0.1 mol% **A**/$FeCl_3$, affords **RO** as a colorless precipitate in 90% yield after 16 h. However, filtering and recharging the solution with xanthene and TBHP led to no further conversion of the substrate. In contrast, the catalyst was much more stable at very low loading and could be recycled multiple times. The reaction between xanthene and 4 eq. of TBHP, catalyzed by 0.002 mol% **A**/$FeCl_3$ was monitored by ^{1}H NMR spectroscopy (Figure 4, top). Under these conditions the catalyst is surprisingly active with 90% conversion of the substrate in 30 h; the TOF at 50% conversion is high at 1595 h^{-1}. Under low-catalyst conditions, **RO** does not precipitate, and instead **ROOtBu** is formed as the major product (78% selectivity at 30 h). The reaction is slower in the second cycle but 80% conversion of xanthene is achieved after an additional 96 h. In the third cycle, the catalyst activity depreciates significantly and only 13% conversion is seen in the next 48 h. Nevertheless, the mixed-metal catalyst is able to carry out more than 100,000 turn-overs under these conditions. Steady catalyst deactivation is seen over time, with the TOF diminishing by approximately 100 h^{-1} every 10 h (Figure 4, bottom).

To investigate the role of $FeCl_3$, a catalytic reaction was carried out using **A** (0.1 mol%) and $InCl_3$ (0.5 mol%) as a chloride-containing, redox-inactive Lewis acid. After 24 h, the room-temperature reaction between xanthene and TBHP (2 eq) shows only 3% conversion. A similar reaction involving scandium(III) triflate (0.5 mol%) achieves higher conversion of 18% after 24 h, forming **ROOtBu** as the sole product. Under the same conditions, reactions involving **A** and $FeCl_3$ achieve 90% conversion at lower catalyst loading (0.1 mol%), yielding higher amounts of the alcohol and ketone products, in just 3 h. These experiments indicate that $FeCl_3$ does not simply act as a Lewis acid or a chloride source, but that its redox properties may also be important.

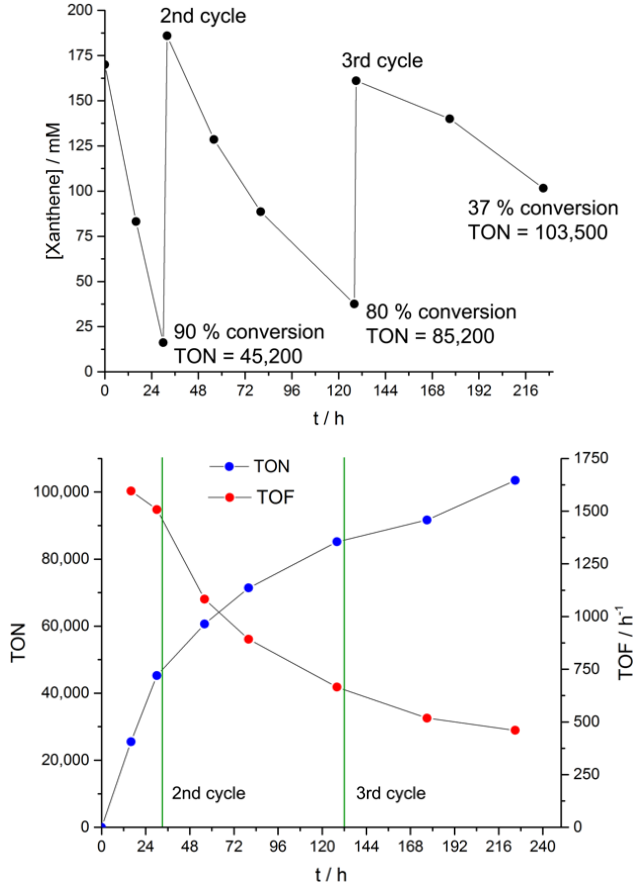

Figure 4. Assessing the stability of the **A**/$FeCl_3$ catalyst in the xanthene oxygenation reaction through multiple reaction cycles. Reaction conditions: stirring d_3-MeCN, room temperature, $[xanthene]_0$ = 170 mM, $[TBHP]_0$ = 680 mM, $[\mathbf{A}]_0$ = 3.4 μM, $[FeCl_3]_0$ = 3.4 μM (0.002 mol%). Top: monitoring the xanthene concentration by ^{1}H NMR spectroscopy to determine the %conversion and TON. Bottom: monitoring changes in TON and TOF during the course of the reaction. Interpolation between the data-points is provided solely as an aid to the eye.

$CuCl_2$ is known to catalyze the oxygenation of benzylic substrates[36] and we find that the room-temperature oxygenation of xanthene by TBHP, catalyzed by $CuCl_2$, proceeds with a reaction profile almost identical to catalytic reactions involving **A**/$FeCl_3$. However, an equimolar mixture of $FeCl_3$ and $CuCl_2$ leads to no enhancement of the $CuCl_2$ catalyzed reaction, indicating that the improved activity and stability of complex **A** on addition of $FeCl_3$ is a direct consequence of the macrocyclic ligand.

Scope of the catalytic reaction

The catalytic reaction is found to be tolerant of the choice of solvent, with identical conversion and product distributions seen after 2 h in acetonitrile (polar, coordinating), dichloromethane (polar, non-coordinating), and benzene (apolar).

A number of peroxide oxidants were tested in the xanthene oxygenation reaction, although TBHP is the best by far (Figure 5). Where 100% conversion of xanthene is seen after 2 h when TBHP is used, the conversion is lowered to 60% when H_2O_2 is used. Use of the organo-peroxides di-*tert*-butyl peroxide (DTBP), *tert*-butyl peroxy-benzoate, or dicumyl peroxide gives no reaction. Similarly, no reaction is seen when carried out in air in the absence of a hydroperoxide oxidant. Finally, adding cyclohexanecarboxaldehyde as a co-oxidant to promote aerobic oxidation[103-104] does not yield any oxygenated products.

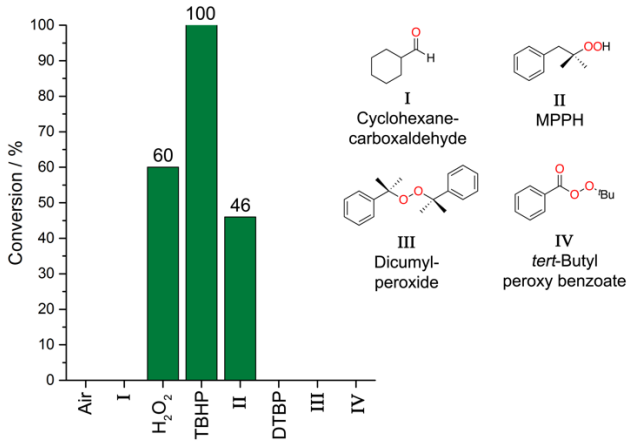

Figure 5. Screening different oxidants in the xanthene oxygenation reaction, catalysed by 0.1 mol% **A** and 0.1 mol% $FeCl_3$. Reaction conditions: 0.15 M xanthene, 2 eq oxidant, stirred MeCN, room temperature, 3 h (conversion of xanthene determined by ^{1}H NMR spectroscopy).

A range of hydrocarbon substrates were tested in reactions with TBHP, catalyzed by **A** only, at loadings between 0.2 and 0.1 mol%. No reaction occurs with cyclohexane[105] or *n*-decanol.[106] Only trace amounts of oxygenated products are seen with cyclohexene,[105] namely cyclohexene oxide, cyclohexenol and cyclohexenone. The aromatic alkene, *trans*-stilbene, reacts to yield the epoxide in 72% selectivity and 97% conversion; 17% of the remaining products are benzaldehyde and benzoic acid, which result from C–C bond breaking. Neither the Baeyer-Villiger reaction of cyclopentanone,[107] nor the oxidation or oxidative-coupling of the *ortho*-directed phenol, 2,4-di-*tert*-butyl phenol,[108-110] are catalyzed by **A**. Similarly, the *para*-directed phenol, 2,6-di-*tert*-butyl phenol does not react to give the expected *para*-quinone or diphenoquinone products.[111-112] Application of the mixed-metal system of **A** and $FeCl_3$ does not improve on any of these reactions.

As the catalytic reaction involving **A** and $FeCl_3$ is restricted mainly to π-activated benzylic substrates, a wider screening of these substrates was undertaken (Scheme 3). The reactions were assessed by ^{1}H NMR spectroscopy and GC-MS, and in some cases were carried out on a preparative scale to isolate the products by column chromatography (Figure 6).

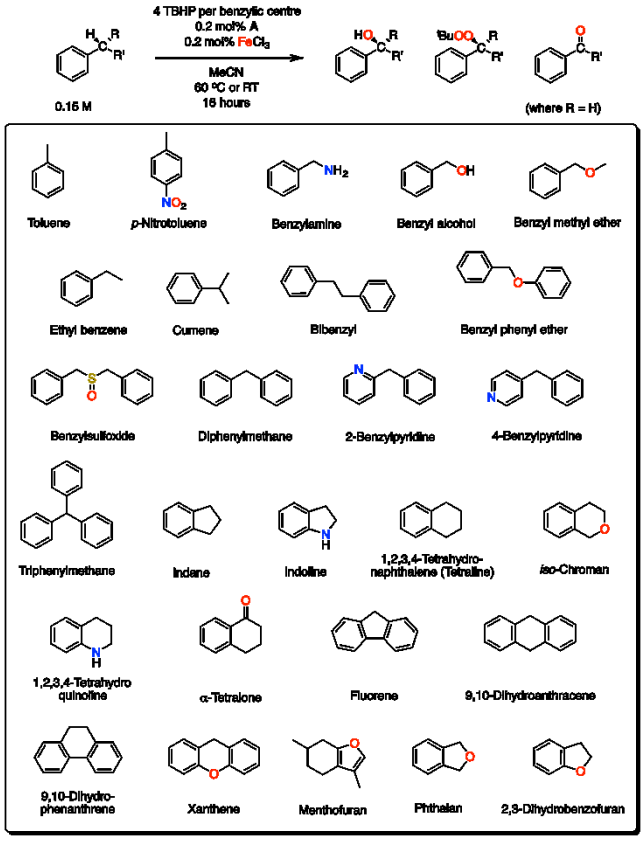

Scheme 3. General reaction and a list of π-activated benzylic substrates tested in the Cu^{II}/Fe^{III}-catalyzed oxygenation reaction.

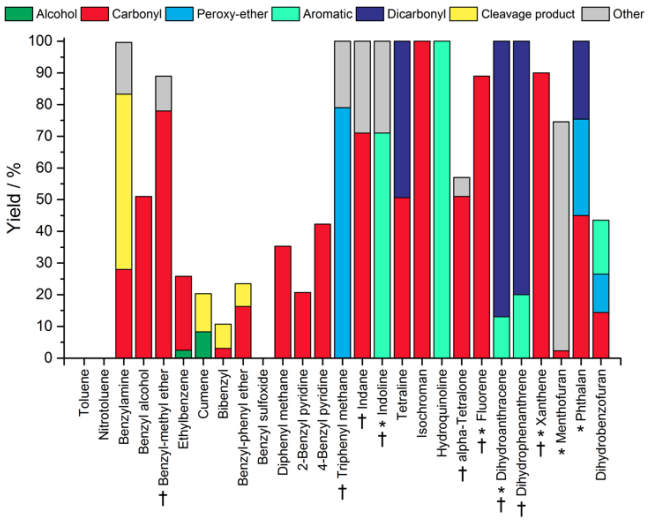

Figure 6. Application of the mixed-metal **A**/$FeCl_3$ catalytic system to a range of π-activated benzylic hydrocarbon substrates. Reaction conditions: 0.15 M substrate, 4 eq TBHP per benzylic position, 0.2 mol% **A**, 0.2 mol% $FeCl_3$, stirred MeCN, 60 °C, 16 h (yields determined by GC-MS using mesitylene as an internal standard). *Reaction carried out at room temperature. †Isolated yields reported after performing the reaction on a 1 mmol scale and purifying by column chromatography.

First, a series of simple substituted benzylic substrates was tested at catalyst loadings of 0.2 mol%, with heating at 60 °C for 16 h. The substrates with high benzylic C–H BDEs, i.e. toluene, *para*-nitro-toluene and benzyl sulfoxide, are not oxidized. Low to moderate conversion is seen for benzyl alcohol (51%), ethyl benzene (26%), cumene (20%), bibenzyl (11%), benzyl phenyl ether (24%), diphenyl methane (3%), 2-benzyl pyridine (21%), and 4-benzyl pyridine (42%). Of these, a few yield single carbonyl products with high selectivity: benzyl alcohol affords benzaldehyde (100%); ethyl benzene affords acetophenone (90%); benzyl-phenyl ether affords phenyl benzoate (69%); diphenyl methane affords benzophenone (100%); and both 2- and 4-benzyl pyridines afford the corresponding benzoyl pyridines (100%). Three substrates in particular underwent high conversion. Benzyl amine is consumed quantitatively, but only affords 28% of the carbonyl product (benzyl amide), with benzaldehyde (55%) and benzonitrile (16%) seen as the other products. Benzyl methyl ether undergoes 91% conversion and is 94% selective for the ester, methyl benzoate. Triphenylmethane also undergoes 100% conversion, and affords (*tert*-butyl)triphenyl methyl peroxy-ether as the sole product.

A series of bicyclic benzylic substrates were tested, all of which undergo high conversion, with the exception of α-tetralone (40%). The *N*-heterocyclic compounds indoline and 1,2,3,4-tetrahydroquinoline both afford the aromatic compounds indole and quinolone quantitatively, with no oxygenation of the substrate taking place following HAA. In contrast, the O-containing heterocycle *iso*-chroman quantitatively affords the mono-ketone product 4-chromanone. Likewise, 94% of indane reacts to afford the mono-ketone, indanone with 89% selectivity. For 1,2,3,4-tetrahydronaphthalene, 100% of the substrate is converted, forming a mixture of the mono-ketone, α-tetralone (51%) and *para*-quinone products 1,4-naphthoquinone (9.5%) and 2,3-dihydro-1,4-naphthoquinone.

The tricyclic benzylic substrates xanthene, fluorene, 9,10-dihydroanthracene (DHA), and 9,10-dihydrophenanthrene were all screened on a preparative scale. All four substrates react with 100% conversion, and the carbonyl products are isolated in high yields: xanthone, 90%; fluorenone, 89%; anthraquinone, 87%; and phenanthraquinone, 80%. Only 9,10-dihydrophenanthrene required heating at 60 °C.

Finally, three furan derivatives of benzylic substrates were tested, as this would hold some relevance to natural product synthesis.[113-114] Phthalan reacts quantitatively at room temperature, with 45% selectivity for the mono-ketone, phthalide. A second product was also formed in significant quantity (representing 30% of the total GC trace). Dihydrobenzofuran only undergoes 44% conversion at 60 °C, to give a mixture of products; benzofuran is identified as the major product at 39% selectivity. Finally, menthofuran undergoes 75% conversion, but the products could not be identified by GC-MS and the selectivity for the major product is low at 34%.

The benzylic substrates that were screened span a benzylic C–H BDE range between 75 and 105 kcal mol^{-1}. Whilst that with the lowest BDE (xanthene) undergoes full conversion, and that with the highest BDE (toluene) does not react, there is no linear correlation between %conversion and BDE between these extremes. Likewise, there is neither correlation between %conversion and benzylic C–H pK_a nor with the ionization energies of the substrates. Comparing a set of substituted benzylic substrates of similar BDE values (85 – 87.5 kcal mol^{-1}) reveals that even in a narrow BDE range, there are vast differences in

%conversion, which is ascribed to functional group sensitivity. The two alkyl-substituted substrates in this sub-set, ethyl benzene and cumene, undergo similar conversion at 26% and 22%, respectively. In comparison, the conversion of benzyl alcohol is higher (57%) and that of benzylamine is higher still (100%). On the other hand, the two ether-containing compounds undergo very different conversions, at 33% for benzyl-phenyl ether and 81% for benzyl-methyl ether.

Characterization of the catalyst

Due to the strong paramagnetism exhibited by both complex **A** and $FeCl_3$, structural characterization of the catalytically-active species by NMR spectroscopy was not possible. Furthermore, we were unable to grow single crystals of the (pre-)catalyst from a wide range of solvent combinations and crystallization conditions and, as such, the structure has not been determined by X-ray crystallography.

It was thought that addition of $FeCl_3$ to **A** might cause: (i) trans-metalation to dinuclear Fe^{III} or heterodinuclear Cu^{II}/Fe^{III} complexes; (ii) the formation of an ate-complex, with $FeCl_3/FeCl_4^-$ incorporated within the Cu^{II} macrocycle through one or more bridging chloride ligands (see Figure 1), reminiscent of dinuclear Zn^{II} macrocycles that bind chloride in the macrocyclic cleft;[115] (iii) the formation of $CuCl_2$ which has been shown to catalyze the oxygenation reaction (see above).

In the +ve ion ESI-MS spectrum of a 1:1 mixture of **A** and $FeCl_3$ in MeCN, no ions corresponding to trans-metalated products are seen. Significantly however, a low-intensity ion at 980 *m/z* is assigned to the ate-complex $[\mathbf{A}\text{-}FeCl_4]^+$ (Figure 7) which might arise from an **A**/$FeCl_3$ complex or alternatively, as $FeCl_3$ is known to form $[FeCl_2(MeCN)_4]^+[FeCl_4]^-$ in MeCN,[116] the formation of an adduct between **A** and the $[FeCl_4]^-$ anion. A further ion is seen at 853 *m/z* consistent with $[\mathbf{A}(Cl)_2]^+$ and supports the ability of the Cu^{II} centers to bind chloride in the presence of $FeCl_3$. The base peak at 697 *m/z* is assigned to $[KH_4L]^+$ and its observation may suggest demetalation and formation of $CuCl_2$.

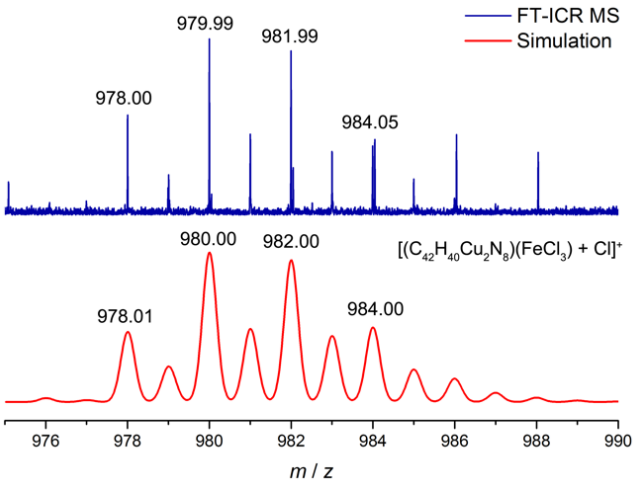

Figure 7. FT-ICR positive ion ESI-MS mass spectrum of a 1:1 solution of **A** and $FeCl_3$ in CH_3CN showing the highest molecular ion peak only (simulated spectrum below).

The electronic absorption spectrum of **A** in MeCN shows three absorption bands at 240, 298 and 367 nm, as well as a shoulder at 400 nm (Figure 8). These are assigned to a mixture of charge-transfer and π- π* transitions and, with ε_{max} of 30,000 $dm^3\ mol^{-1}\ cm^{-1}$ (at 240 nm), these bands would obscure the low-intensity charge-transfer bands of $CuCl_2$ and $FeCl_3$ (ε_{max} = 2,700 at 310 nm for $CuCl_2$; 8,300 at 240 nm for $FeCl_3$). Nonetheless, the absorption spectrum of **A**/$FeCl_3$ in MeCN is near-identical to that of **A** and does not support demetalation.

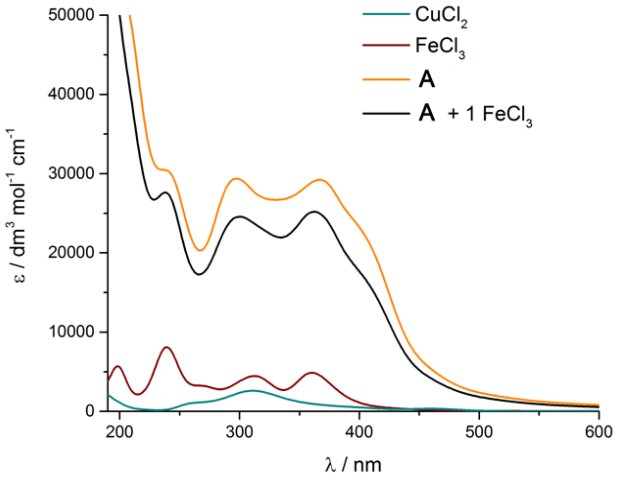

Figure 8. Electronic absorption spectra for $CuCl_2$, $FeCl_3$, **A**, and **A**/$FeCl_3$ at equimolar concentration in MeCN.

In the cyclic voltammogram (CV) **A** undergoes two irreversible Cu^{II}/Cu^{I} reduction processes at E_p^c –1.40 and –1.71 V vs. Fc^+/Fc, and two irreversible Cu^{III}/Cu^{II} oxidation processes at E_p^a +0.36 and +0.60 V (Figure S55). These step-wise redox processes indicate that electronic communication between the two metal centers occurs and is consistent with its EPR spectrum (see below). $FeCl_3$ undergoes irreversible Fe^{III}/Fe^{II} reduction at E_p^c –0.56 V, and $CuCl_2$ undergoes reversible Cu^{III}/Cu^{II} oxidation at $E_{1/2}$ +0.11 V, with the cathodic wave appearing at E_p^c +0.05 V. In **A**/$FeCl_3$, a new, irreversible cathodic wave is seen in the CV, at E_p^c –0.31 V, approximately midway between the cathodic waves of $CuCl_2$ and $FeCl_3$ (Figure S56). The peak-height of this new wave is directly proportional to the concentration of $FeCl_3$, and increases steadily on addition of $FeCl_3$ in portions (Figure S57). In the square-wave voltammogram of the mixture (SWV, Figure 9), it is more apparent that this new reduction process (E_p^c –0.29 V), with its lower-intensity anodic wave on the return scan (E_p^a –0.15 V), resembles the SWV signal of $FeCl_3$, albeit 166 mV more positive than for $FeCl_3$ measured in isolation. The presence of even trace amounts $CuCl_2$ would be immediately obvious in the SWV, due to the nanomolar detection limit inherent with that technique.[117-119] The 166 mV anodic shift of the $FeCl_3$ reduction wave in the SWV is also accompanied by a 44 – 88 mV cathodic shift in the oxidation waves for **A**, and therefore lends support to the formation of a Cu^{II}/Fe^{III} ate-complex.

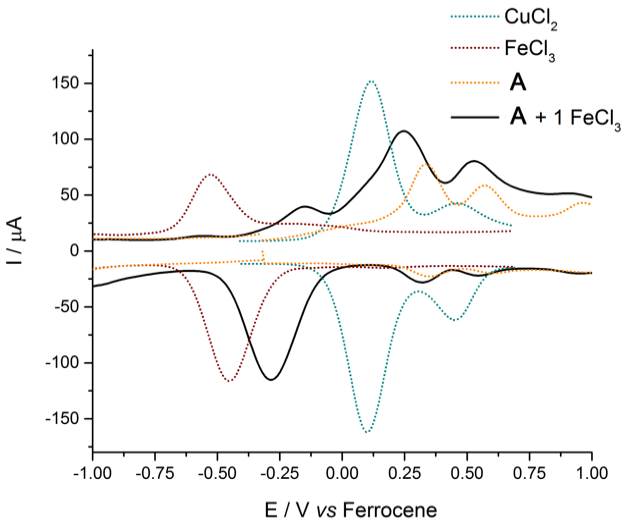

Figure 9. Square-wave voltammograms for $CuCl_2$, $FeCl_3$, **A**, and **A**/$FeCl_3$. All measured at 124 mV s^{-1} as 1 mM MeCN solutions in 0.1 M [^{n}Bu$_4$N][PF_6], using a glassy-carbon working electrode, Pt gauze counter electrode and Ag-wire quasi-reference electrode.

The EPR spectra of dinuclear Cu^{II} Pacman complexes that are structurally similar to **A** have been reported previously.[83] The frozen MeCN/THF solution X-band EPR spectrum of **A** shows a signal consistent with two weakly coupled Cu^{II} ($S = {}^1/_2$) ions (Figure S59).[120-121] The spectral profile is dominated by an axial g splitting synonymous with Cu^{II}, plus addition of the small exchange coupling gives rise to the weakly-resolved 7-line hyperfine pattern at low-field, characteristic of coupled ^{63,65}Cu nuclei ($I = {}^3/_2$, 100% abundant). A signature half-field signal is seen, arising from the forbidden $\Delta M_S = 2$ transition of the spin triplet ($S = 1$) formed by coupling of the two Cu^{II} ions, in agreement with the electrochemical measurements discussed above. The X-band EPR spectrum of $FeCl_3$ measured under the same conditions features a broad single signal with $g = 2$, commensurate with an $S = {}^5/_2$ ferric species with intrinsically minute zero-field splitting.[122] Mixing equimolar amounts of **A** and $FeCl_3$ produces a spectrum consistent with the sum of the two paramagnetic components. The half-field transition is still seen and is unperturbed by the presence of $FeCl_3$. Furthermore, there is no detectable indication of coupling between the Cu^{II} and Fe^{III} centers; the stronger coupling between the two Cu^{II} centers masks any interaction and dominates the spectral profile.

The Fourier transform of the EXAFS region of the Cu K-edge X-ray absorption spectrum for **A** measured in MeCN at 95 K (Figure 10) is well-reproduced using the crystal structure metrics (Table S5). Crystallographic Cu–N distances in the first coordination sphere are 1.903(2) and 1.919(3) Å for pyrrolide donors, and 1.987(2) and 2.073(3) Å for imine donors and compare well with the fitted EXAFS predicted Cu–N distances of 1.926, 2.016 and 2.066 Å, respectively. The Cu···Cu separation of 3.95 Å in the EXAFS is slightly longer than that determined crystallographically (3.6157(6) Å), but in close agreement with the distance previously determined by EPR in frozen solution (3.8 Å).[83] Cu K-edge EXAFS recorded after addition of $FeCl_3$ to **A** (Figure 10) further show that the Cu ion remains complexed by the macrocycle. A prominent scattering peak evident in the Fourier transform was modelled by including a single Cl atom from $FeCl_3/FeCl_4^-$. The best fit places this Cl atom 3.524 Å away from Cu (Table S6). As such, the EPR and EXAFS data indicate that **A** and $FeCl_3/FeCl_4^-$ form a weakly-associated adduct in solution rather than a formal ate-complex (Figure 1). Formation of such a hetero-metallic adduct, resulting in improved catalytic activity, is likely directed by the macrocyclic setting.

The XANES spectra at the Cu K-edge are dominated by the effective nuclear charge at Cu, and in this case are persistently Cu^{II}. The edge position is unaffected by the inclusion of $FeCl_3$, and furthermore, the potential changes to the coordination sphere about Cu from local square-planar to pyramidal geometry due to the presence of Cl have no bearing on the pre-edge profile, with no departure from centrosymmetry. The pre-edge feature is small and like other Cu K-edge data, is observed as small bump or shoulder at the foot of the white line, yielding little information.

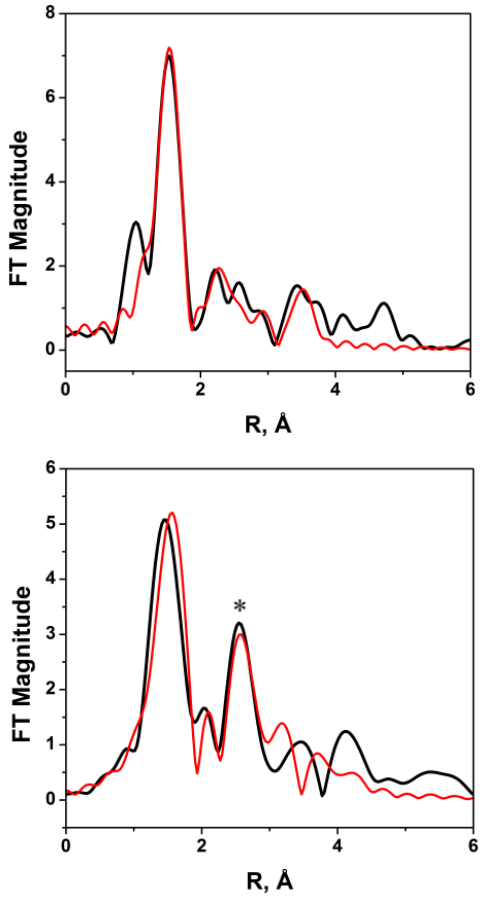

Figure 10. EXAFS for complex **A** (top) and a 1:1 mixture of **A** and $FeCl_3$ (bottom) following Fourier transform. Measured as MeCN solutions at 95 K. Experimental data are black; simulations are red. The asterisk marks the new peak observed following addition of $FeCl_3$.

Attempts were made to identify the product of reactions between either **A** or **A**/$FeCl_3$ and TBHP. In all cases, we were unable to isolate any pure material, with reactions often leading to biphasic mixtures of oily residues. All crystallization attempts were unsuccessful. In contrast, the +ion ESI-MS of the reaction between **A** and an excess of TBHP shows an ion at m/z 873 that is consistent with the formation of an **A**(TBHP) complex (Figure S48), in which we surmise that the TBHP is bound within

the macrocyclic cleft. Unfortunately, no further evidence of potentially catalytically active species, especially in the presence of $FeCl_3$, could be gained.

Reaction mechanism, initial rates and simulation of pathways

The nature of catalytic hydrocarbon oxygenation reactions remains contentious as to whether the reaction proceeds through a reactive metal complex or freely-diffusing radicals. A number of iron-oxo complexes were once thought to carry out HAA and oxygenation of substrates (Gif chemistry),[123-125] but HAA was later attributed to hydroxyl radicals, that in turn formed organic radicals (i.e. Fenton chemistry).[126-129] The oxygenation was shown by isotopic labelling[130-131] and argon purge experiments[100] to proceed through an auto-oxidation mechanism involving O_2.

The formation of highly reactive, freely-diffusing hydroxyl, *tert*-butoxyl or *tert*-butylperoxyl radicals should lead to HAA from substrates with high C–H BDEs, such as toluene or cyclohexane. However, no reactions with these substrates were observed during this work. Furthermore, the rate of the decomposition reaction of the free *tert*-butoxyl radical by β-scission is rapid ($k = 2.1 \times 10^4$ s^{-1}).[132] Thus the generation of *tert*-butanol as a co-product from the reactions studied herein indicates that if a *tert*-butoxyl radical is present, it is closely-associated with, and stabilized by, the catalyst.

Concerning the radical nature of the substrate following HAA, quantitative conversion of dihydroanthracene, DHA, is seen with high selectivity for anthraquinone (90%) over anthracene (10%). Similarly, the reaction of 9,10-dihydrophenanthrene produces phenanthraquinone in 80% yield. In a reaction mechanism that involves freely-diffusing benzylic radicals, anthracene or phenanthrene would be expected as the sole products.

Reactions catalyzed by **A** at 80 °C, or by **A**/$FeCl_3$ at room temperature, are unaffected by the presence of O_2, with identical yields of oxygenated xanthene products seen from reactions carried out under air or N_2. In contrast to previous studies, no homo-coupled 9,9'-bixanthene product is seen, even when the reaction is carried out under N_2.[100] This provides further evidence that freely-diffusing organic radicals are not present, and also indicates that the hydroperoxide is responsible for oxygenation of the substrate, rather than O_2 through an auto-catalysis radical mechanism.

Assertions in the literature claim that high selectivity for peroxy-ether and ketone products is a signature for a free-radical mechanism.[133] Whilst we have observed high selectivities for these products in our work, our other observations show that the HAA and oxygenation steps do not result from free radicals. As such, the mechanistic probe, 2-methyl-1-phenylpropan-2-yl hydroperoxide (MPPH) was used[134] as, in this case, the alkoxyl free-radical formed following homolytic O–O bond fission in MPPH is unstable and undergoes very rapid β-scission, forming acetone and benzyl radical ($k \sim 2.2 \times 10^8$ s^{-1}). In the case of a free-radical mechanism, the only products from a reaction involving xanthene and MPPH should therefore be acetone and those derived from benzyl free radicals. The room temperature reaction between xanthene and 1 eq of MPPH catalyzed by 0.1 mol% **A**/$FeCl_3$ (Scheme 4) results in 90% conversion of xanthene, whilst that with 2 eq of MPPH results in quantitative conversion. In line with the TBHP reactions above, the stoichiometry of MPPH influences the product distribution; use of 1 eq of MPPH gives **ROH** (30%), peroxy-ether (37%) and **RO** (33%) whereas 2 eq of MPPH gives **ROH** (6%), peroxy-ether (52%) and **RO** (42%).

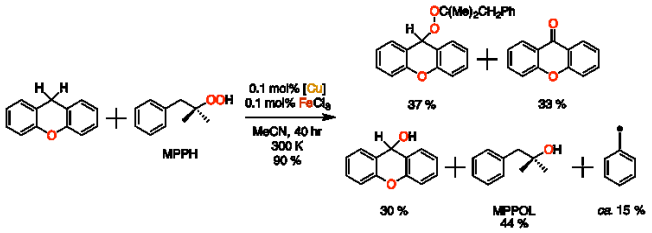

Scheme 4. Reaction of xanthene with one equivalent of MPPH. Selectivities / % for xanthene oxidation products are with respect to xanthene. Selectivities / % for MPPOL and benzyl radical-derived products are with respect to MPPH.

Significantly, a resonance for the benzylic proton of 2-methyl-1-phenylpropan-2-ol (MPPOL) is seen at 2.72 ppm in the ^{1}H NMR spectrum, in a ratio of 4:5 with MPPH. The presence of significant amounts of MPPOL supports a *metal-associated* mechanism, as coordination of the alkoxide or alkoxyl radical to a metal center stabilizes the radical against β-scission. Furthermore, the presence of unreacted MPPH indicates that a *metal hydroxide* is also responsible for HAA, in order to account for the 90% conversion of the xanthene substrate. However, analysis of the reaction mixtures involving MPPH by GC-MS reveals that the benzyl-radical derived products benzaldehyde, benzyl alcohol and bibenzyl are also formed, albeit in low concentration (approximately 15% compared with xanthene). Overall, a predominantly metal-associated mechanism best fits with the observations above.

It is therefore apparent that the oxygenation reactions catalyzed by **A**/$FeCl_3$ feature elements of both free-radical and radical-free mechanisms.[48,54,135] We therefore suggest that the reaction mechanism in this work involves "well-disguised", metal-associated radical species,[8-10,133] in which the organic radical of the substrate that is formed following HAA is associated with the intermediate as a "cage-radical".[136]

To further elucidate the reaction pathways for the overall oxidation process, the reaction kinetics were explored *in situ* by ^{1}H NMR spectroscopy. Under the standard reaction conditions employed earlier (0.15 M xanthene, 0.30 M TBHP, 0.1 mol% **A** and 0.1 mol% $FeCl_3$), the xanthene consumption approximately fitted to a first-order integrated rate law, albeit coincidently (see below). Deuteration of xanthene at the benzylic 9-position slows the rate of xanthene consumption marginally (Figure 11, Figure S95), indicative of a small primary kinetic isotope effect (KIE, $\nu_H/\nu_D = 1.5$). Deuteration has a pronounced impact on the product distribution, with a substantial KIE estimated for the conversion of xanthyl peroxide into xanthydrol / ketone ($\nu_H/\nu_D \approx 6$). Deuteration at the 9-position of xanthene therefore has a more pronounced effect on the second oxidation step(s). The oxygenation reaction of d_2-xanthene was also monitored by ^{2}H NMR spectroscopy (Figure S96), which confirms that *t*BuOD forms as a co-product. No D_2O / HDO was detected.

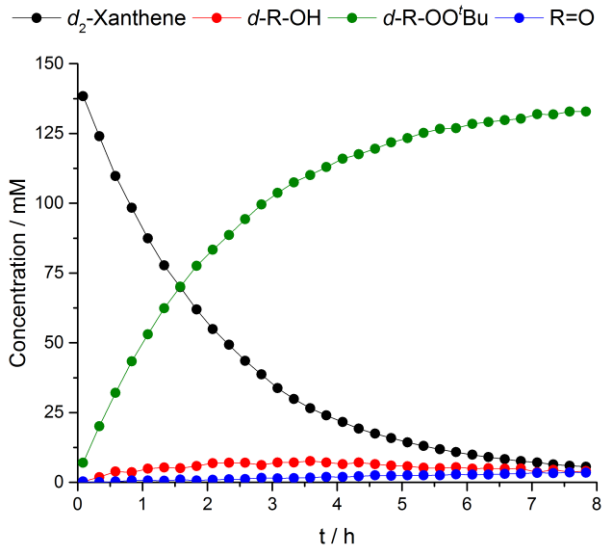

Figure 11. Monitoring oxygenation of d_2-xanthene by 4 eq TBHP, catalysed by 0.1 mol% **A** and 0.1 mol% $FeCl_3$ at 300 K in d_3-MeCN (concentrations determined by ^{1}H NMR integration). Interpolation between the data-points is provided solely as an aid to the eye.

The influence of the electronic properties of the substrate on the rate of the reaction was briefly investigated using a series of xanthene substrates substituted at the 2-position, (see Figure S97). The reaction constant, ρ, is small but positive (1.2 ± 0.2), implying only marginal accumulation of electron density at the benzylic reaction center, and is consistent with both radical and radical-free mechanisms.[137-138]

In order to further explore the system, the reactant concentrations were varied from the standard conditions. However, this rapidly led to major deviations from what had appeared as approximately first-order kinetics; indeed, no simple correlations were evident. Initial rates were thus analyzed as a function of all components (xanthene, TBHP, **A** and $FeCl_3$) which were independently varied. The initial rate was found to have a linear dependency on the initial concentrations of xanthene (albeit with a small non-zero intercept), the copper catalyst (**A**) and the $FeCl_3$, suggesting first order kinetics with respect to each component (Figures S98, S100 and S101). Importantly, the initial rates become independent of copper catalyst (**A**) and $FeCl_3$ when the concentration of one pre-catalyst becomes super-stoichiometric over the other. In other words, **A** and $FeCl_3$ appear to operate cooperatively (1:1 ratio). The initial rate as a function of the TBHP concentration was approximately first order at low concentrations, becoming independent above approximately 200 mM, indicative of saturation in this reagent (Figure S99).

The temporal evolution of the xanthene oxygenation reaction, from a series of around 40 experiments in which the initial concentrations of reactants was varied, was qualitatively analyzed to identify trends and relationships between components. Three important features arose from these studies:

(i) The concentration of **ROOtBu** reaches a maximum value at the point that the xanthene substrate is entirely consumed. After this it is converted to ketone (**RO**) indicative of competition between xanthene and **ROOtBu** for the catalyst or a reactive intermediate.

(ii) **ROH** and **ROOtBu** form at identical rates when the initial concentrations of xanthene and TBHP are equimolar. Increasing the ratio of [TBHP] / [xanthene] results in **ROOtBu** being formed at a faster rate than **ROH**, indicating that **ROOtBu** and **ROH** arise from separate pathways or intermediates.

(iii) In cases where there is sufficient oxidant for conversion of **ROH** / **ROOtBu** to ketone (**RO**), the concentration of the alcohol (**ROH**) reaches a maximum shortly after the point where [xanthene] = [**ROOtBu**]. This final aspect was explored in a more quantitative way, by co-plotting temporal concentrations of xanthene, **ROH** and **ROOtBu** (see Figures S102 to S107 and Table S6).

The three features outlined above were then employed as the starting point for a series of models for reaction pathways that might account for the overall transformations. Extensive kinetic simulations were conducted to explore a very diverse series of models of increasing complexity. The failure of any of these models to provide a satisfactory global fit to the entire data-set (40 experiments) is indicative of the complex and interlinked nature of the reaction pathways. Nonetheless, the most effective model tested (outlined schematically in Scheme 5, full details provided in the SI) is able to provide a qualitative tool for prediction of temporal product distributions as a function of all initial concentrations. Consistent with the complexity of the system, and the qualitative nature of the model, some initial sets of conditions give better fits than others; two examples are given in Figure 12.

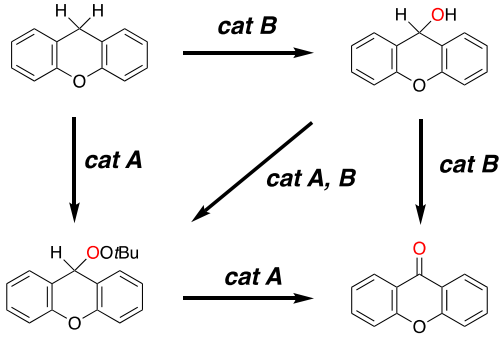

Scheme 5. Schematic representation of the reaction network employed to explore the kinetics of oxidation of xanthene, catalyzed by a mixture of complex **A** and $FeCl_3$. Each step in the network involves the exogenous oxidant (TBHP). The primary catalyst initially generated from **A** + $FeCl_3$ is represented as **cat A**; a secondary, higher oxidation state species, generated by branching from the primary catalytic cycle is represented as **cat B**. Not shown in the network is an irreversible oxidative degradation of the primary catalyst and its reversible inhibition by xanthone complexation - see SI for full details.

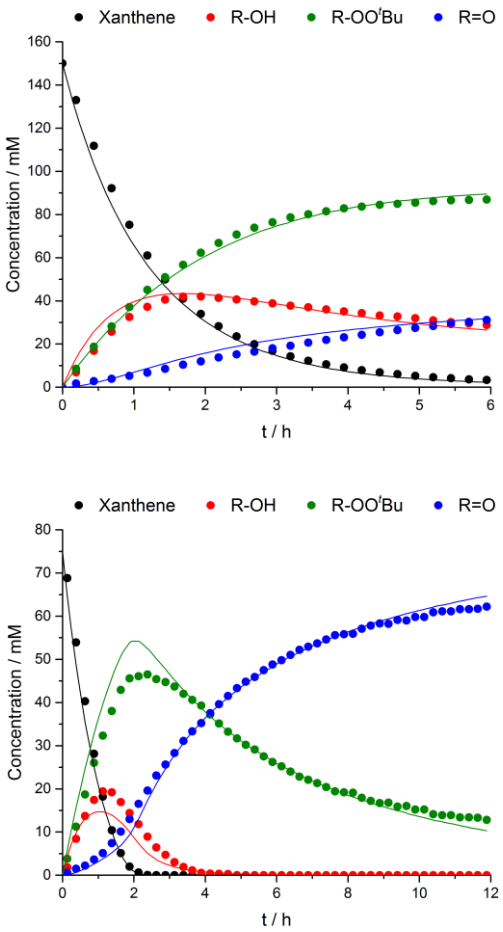

Figure 12. Simulation of the xanthene oxygenation reaction, catalyzed by **A**/$FeCl_3$, using the generalized reaction pathway presented in Scheme 5 (full details in Scheme S1). Top: $[xanthene]_0$ = 150 mM, $[TBHP]_0$ = 300 mM, $[\mathbf{A}]_0$ = 150 µM, $[FeCl_3]_0$ = 150 µM. Bottom: $[xanthene]_0$ = 75 mM, $[TBHP]_0$ = 300 mM, $[\mathbf{A}]_0$ = 150 µM, $[FeCl_3]_0$ = 150 µM. Simulated data plotted as solid curves, experimental data plotted as dots.

Conclusions

The dinuclear copper(II) complexes **A** – **C** catalyze the oxygenation of hydrocarbon substrates using hydroperoxide oxidants at elevated temperature. Whilst these complexes undergo rapid deactivation, addition of $FeCl_3$ improves the catalyst stability and efficacy, resulting in much higher turn-over numbers and allowing the reaction to proceed at room temperature. A combined spectroscopic and voltammetric study indicates that the catalyst is likely a weakly-associated adduct, with an $FeCl_3$ or $FeCl_4^-$ moiety bound within the macrocyclic cleft. It is the macrocyclic ligand that encourages cooperative action between Cu^{II} and Fe^{III} in the oxygenation reaction, which is a novel strategy in oxidation catalysis.

The catalytic reaction involving **A**/$FeCl_3$ is limited to π-activated benzylic substrates, achieving oxygenation in high conversion for those with low to moderate C–H BDEs. Observation of oxygenated products indicates that a non-radical mechanism is operative, which is reinforced by N_2-purge experiments and the use of a MPPH mechanistic probe. However, the high selectivity for ketone, small KIE, and Hammett analysis indicate that the mechanism features radical elements, and the mechanism is therefore thought to be driven by metal-associated radicals.

Whilst the initial rates study that was conducted did not provide definitive insight into the reaction mechanism, a possible, albeit complex reaction network (Scheme 5) has been deduced through the analysis of qualitative trends and kinetic modelling. This is presented in its current form to illustrate the complexity of the kinetics of the reaction catalyzed by **A**/$FeCl_3$ and as a basis for more detailed mechanistic work in the future.

ASSOCIATED CONTENT

The Supporting Information is available free of charge on the ACS Publications website at http://pubs.acs.org. Full experimental details, catalysis procedures, substrate screening data, mass spectra, UV/vis data, cyclic voltammetry, EPR data, EXAFS analysis and full kinetic data.

AUTHOR INFORMATION

Corresponding Authors

* J.B.L.: jason.love@ed.ac.uk. G.C.L.J.: guy.lloyd-jones@ed.ac.uk. S.S.: stephen.sproules@glasgow.ac.uk

Author Contributions

The manuscript was written through contributions of all authors.

Funding Sources

We thank the University of Edinburgh for the award of a Principal's Career Development Scholarship (Ph.D. studentship to J.R.P.) and the EPSRC CRITICAT Centre for Doctoral Training (Ph.D. studentship to M.C.; Grant code: EP/L016419/1) for financial support. The research leading to these results has received funding from the European Research Council under the European Union's Seventh Framework Programme (FP7/2007-2013) / ERC grant agreement n° [340163]. We thank the Diamond Light Source for the data collected on beamline B18 (Rapid Access Proposal Number SP15756).

ACKNOWLEDGMENT

We also thank Dr Lorna Murray for NMR support and Dr Logan Mackay for mass spectrometry support.

REFERENCES

(1) Wallar, B. J.; Lipscomb, J. D. Dioxygen Activation by Enzymes Containing Binuclear Non-Heme Iron Clusters, *Chem. Rev.* **1996**, *96*, 2625.

(2) Que, L.; Ho, R. Y. N. Dioxygen Activation by Enzymes with Mononuclear Non-Heme Iron Active Sites, *Chem. Rev.* **1996**, *96*, 2607.

(3) Sono, M.; Roach, M. P.; Coulter, E. D.; Dawson, J. H. Heme-Containing Oxygenases, *Chem. Rev.* **1996**, *96*, 2841.

(4) Solomon, E. I.; Sundaram, U. M.; Machonkin, T. E. Multicopper Oxidases and Oxygenases, *Chem. Rev.* **1996**, *96*, 2563.

(5) Basu, P.; Katterle, B.; Andersson, K. K.; Dalton, H. The membrane-associated form of methane mono-oxygenase from Methylococcus capsulatus (Bath) is a copper/iron protein, *Biochem. J.* **2003**, *369*, 417.

(6) Hemsworth, G. R.; Davies, G. J.; Walton, P. H. Recent insights into copper-containing lytic polysaccharide mono-oxygenases, *Curr. Opin. Struc. Biol.* **2013**, *23*, 660.

(7) Nesterov, D. S.; Nesterova, O. V.; Pombeiro, A. J. L. Homo- and heterometallic polynuclear transition metal catalysts for alkane CH

bonds oxidative functionalization: Recent advances, *Coord. Chem. Rev.* **2017**.

(8) Casadei, C. M.; Gumiero, A.; Metcalfe, C. L.; Murphy, E. J.; Basran, J.; Concilio, M. G.; Teixeira, S. C. M.; Schrader, T. E.; Fielding, A. J.; Ostermann, A.; Blakeley, M. P.; Raven, E. L.; Moody, P. C. E. Neutron cryo-crystallography captures the protonation state of ferryl heme in a peroxidase, *Science* **2014**, *345*, 193.

(9) Groves, J. T. Enzymatic C-H bond activation: Using push to get pull, *Nat. Chem.* **2014**, *6*, 89.

(10) Rittle, J.; Green, M. T. Cytochrome P450 Compound I: Capture, Characterization, and C-H Bond Activation Kinetics, *Science* **2010**, *330*, 933.

(11) Citek, C.; Herres-Pawlis, S.; Stack, T. D. P. Low Temperature Syntheses and Reactivity of Cu_2O_2 Active-Site Models, *Acc. Chem. Res.* **2015**, *48*, 2424.

(12) Ramsden, C. A.; Riley, P. A. Tyrosinase: The four oxidation states of the active site and their relevance to enzymatic activation, oxidation and inactivation, *Bioorg. Med. Chem.* **2014**, *22*, 2388.

(13) Banerjee, R.; Proshlyakov, Y.; Lipscomb, J. D.; Proshlyakov, D. A. Structure of the key species in the enzymatic oxidation of methane to methanol, *Nature* **2015**, *518*, 431.

(14) Culpepper, M. A.; Cutsail, G. E.; Hoffman, B. M.; Rosenzweig, A. C. Evidence for Oxygen Binding at the Active Site of Particulate Methane Monooxygenase, *J. Am. Chem. Soc.* **2012**, *134*, 7640.

(15) Rosenzweig, A. C. Biochemistry: Breaking methane, *Nature* **2015**, *518*, 309.

(16) Ervin, K. M.; DeTuri, V. F. Anchoring the Gas-Phase Acidity Scale, *J. Phys. Chem. A* **2002**, *106*, 9947.

(17) Que, L.; Tolman, W. B. Biologically inspired oxidation catalysis, *Nature* **2008**, *455*, 333.

(18) Que, J. L.; Tolman, W. B. Bis(μ-oxo)dimetal "Diamond" Cores in Copper and Iron Complexes Relevant to Biocatalysis, *Angew. Chem. Int. Ed.* **2002**, *41*, 1114.

(19) Holland, P. L.; Cramer, C. J.; Wilkinson, E. C.; Mahapatra, S.; Rodgers, K. R.; Itoh, S.; Taki, M.; Fukuzumi, S.; Que, L.; Tolman, W. B. Resonance Raman Spectroscopy as a Probe of the Bis(μ-oxo)dicopper Core, *J. Am. Chem. Soc.* **2000**, *122*, 792.

(20) Shimizu, K.; Maruyama, R.; Hatamachi, T.; Kodama, T. O2-Bridged Multicopper(II) Complex in Zeolite for Catalytic Direct Photo-oxidation of Benzene to Diphenols, *J. Phys. Chem. C* **2007**, *111*, 6440.

(21) Garcia-Bosch, I.; Cowley, R. E.; Diaz, D. E.; Siegler, M. A.; Nam, W.; Solomon, E. I.; Karlin, K. D. Dioxygen Activation by a Macrocyclic Copper Complex Leads to a Cu_2O_2 Core with Unexpected Structure and Reactivity, *Chem. Eur. J.* **2016**, *22*, 5133.

(22) Rosenthal, J.; Luckett, T. D.; Hodgkiss, J. M.; Nocera, D. G. Photocatalytic Oxidation of Hydrocarbons by a Bis-iron(III)-μ-oxo Pacman Porphyrin Using O_2 and Visible Light, *J. Am. Chem. Soc.* **2006**, *128*, 6546.

(23) Groves, J. T.; Nemo, T. E. Epoxidation reactions catalyzed by iron porphyrins. Oxygen transfer from iodosylbenzene, *J. Am. Chem. Soc.* **1983**, *105*, 5786.

(24) Costas, M. Selective C–H oxidation catalyzed by metalloporphyrins, *Coord. Chem. Rev.* **2011**, *255*, 2912.

(25) Yuan, Y.; Ji, H.; Chen, Y.; Han, Y.; Song, X.; She, Y.; Zhong, R. Oxidation of Cyclohexane to Adipic Acid Using Fe−Porphyrin as a Biomimetic Catalyst, *Org. Process. Res. Dev.* **2004**, *8*, 418.

(26) Nappa, M. J.; Tolman, C. A. Steric and electronic control of iron porphyrin catalyzed hydrocarbon oxidations, *Inorg. Chem.* **1985**, *24*, 4711.

(27) Collman, J. P.; Zhang, X.; Lee, V. J.; Uffelman, E. S.; Brauman, J. I. Epoxidation metalloporphyrins, *Science* **1993**, *261*, 1404.

(28) Nam, W. High-Valent Iron(IV)–Oxo Complexes of Heme and Non-Heme Ligands in Oxygenation Reactions, *Acc. Chem. Res.* **2007**, *40*, 522.

(29) Kim, S. O.; Sastri, C. V.; Seo, M. S.; Kim, J.; Nam, W. Dioxygen Activation and Catalytic Aerobic Oxidation by a Mononuclear Nonheme Iron(II) Complex, *J. Am. Chem. Soc.* **2005**, *127*, 4178.

(30) Kaizer, J.; Klinker, E. J.; Oh, N. Y.; Rohde, J.-U.; Song, W. J.; Stubna, A.; Kim, J.; Münck, E.; Nam, W.; Que, L. Nonheme Fe(IV)=O Complexes That Can Oxidize the C−H Bonds of Cyclohexane at Room Temperature, *J. Am. Chem. Soc.* **2004**, *126*, 472.

(31) Martínez-Ferraté, O.; Britovsek, G. J. P.; Claver, C.; van Leeuwen, P. W. N. M. C–H benzylic oxidation promoted by dinuclear iron DBDOC iminopyridine complexes, *Inorg. Chim. Acta.* **2015**, *431*, 156.

(32) Chen, M. S.; White, M. C. A Predictably Selective Aliphatic C–H Oxidation Reaction for Complex Molecule Synthesis, *Science* **2007**, *318*, 783.

(33) Lyakin, O. Y.; Bryliakov, K. P.; Britovsek, G. J. P.; Talsi, E. P. EPR Spectroscopic Trapping of the Active Species of Nonheme Iron-Catalyzed Oxidation, *J. Am. Chem. Soc.* **2009**, *131*, 10798.

(34) Boess, E.; Wolf, L. M.; Malakar, S.; Salamone, M.; Bietti, M.; Thiel, W.; Klussmann, M. Competitive Hydrogen Atom Transfer to Oxyl- and Peroxyl Radicals in the Cu-Catalyzed Oxidative Coupling of N-Aryl Tetrahydroisoquinolines Using tert-Butyl Hydroperoxide, *ACS Catal.* **2016**, *6*, 3253.

(35) Hossain, M. M.; Shyu, S.-G. Biphasic copper-catalyzed C–H bond activation of arylalkanes to ketones with tert-butyl hydroperoxide in water at room temperature, *Tetrahedron* **2016**, *72*, 4252.

(36) Rothenberg, G.; Feldberg, L.; Wiener, H.; Sasson, Y. Copper-catalyzed homolytic and heterolytic benzylic and allylic oxidation using tert-butyl hydroperoxide, *J. Chem. Soc. Perkin Trans. 2* **1998**, 2429.

(37) Chen, X.; Hao, X.-S.; Goodhue, C. E.; Yu, J.-Q. Cu(II)-Catalyzed Functionalizations of Aryl C−H Bonds Using O_2 as an Oxidant, *J. Am. Chem. Soc.* **2006**, *128*, 6790.

(38) Eames, J.; Watkinson, M. Catalytic Allylic Oxidation of Alkenes Using an Asymmetric Kharasch–Sosnovsky Reaction, *Angew. Chem. Int. Ed.* **2001**, *40*, 3567.

(39) Kharasch, M. S.; Sosnovsky, G. The reactions of t-butyl perbenzoate and olefins—a stereospecific reaction, *J. Am. Chem. Soc.* **1958**, *80*, 756.

(40) Beckwith, A. L. J.; Zavitsas, A. A. Allylic oxidations by peroxy esters catalyzed by copper salts. The potential for stereoselective syntheses, *J. Am. Chem. Soc.* **1986**, *108*, 8230.

(41) Andrus, M. B.; Lashley, J. C. Copper catalyzed allylic oxidation with peresters, *Tetrahedron* **2002**, *58*, 845.

(42) Gephart, R. T.; McMullin, C. L.; Sapiezynski, N. G.; Jang, E. S.; Aguila, M. J. B.; Cundari, T. R.; Warren, T. H. Reaction of CuI with Dialkyl Peroxides: Cu(II)-Alkoxides, Alkoxy Radicals, and Catalytic C–H Etherification, *J. Am. Chem. Soc.* **2012**, *134*, 17350.

(43) Nakanishi, M.; Bolm, C. Iron-Catalyzed Benzylic Oxidation with Aqueous tert-Butyl Hydroperoxide, *Adv. Synth. Catal.* **2007**, *349*, 861.

(44) Enthaler, S.; Junge, K.; Beller, M. Sustainable Metal Catalysis with Iron: From Rust to a Rising Star?, *Angew. Chem. Int. Ed.* **2008**, *47*, 3317.

(45) Shul'pin, G. B.; Golfeto, C. C.; Süss-Fink, G.; Shul'pina, L. S.; Mandelli, D. Alkane oxygenation with H_2O_2 catalysed by $FeCl_3$ and 2,2′-bipyridine, *Tetrahedron Lett.* **2005**, *46*, 4563.

(46) Join, B.; Möller, K.; Ziebart, C.; Schröder, K.; Gördes, D.; Thurow, K.; Spannenberg, A.; Junge, K.; Beller, M. Selective Iron-Catalyzed Oxidation of Benzylic and Allylic Alcohols, *Adv. Synth. Catal.* **2011**, *353*, 3023.

(47) Möller, K.; Wienhöfer, G.; Schröder, K.; Join, B.; Junge, K.; Beller, M. Selective Iron-Catalyzed Oxidation of Phenols and Arenes with Hydrogen Peroxide: Synthesis of Vitamin E Intermediates and Vitamin K3, *Chem. -Eur. J.* **2010**, *16*, 10300.

(48) Shi, F.; Tse, M. K.; Li, Z.; Beller, M. Controlling Iron-Catalyzed Oxidation Reactions: From Non-Selective Radical to Selective Non-Radical Reactions, *Chem. -Eur. J.* **2008**, *14*, 8793.

(49) Li, D.; Schröder, K.; Bitterlich, B.; Tse, M. K.; Beller, M. Iron-catalyzed hydroxylation of β-ketoesters with hydrogen peroxide as oxidant, *Tetrahedron Lett.* **2008**, *49*, 5976.

(50) Gelalcha, F. G.; Bitterlich, B.; Anilkumar, G.; Tse, M. K.; Beller, M. Iron-Catalyzed Asymmetric Epoxidation of Aromatic Alkenes Using Hydrogen Peroxide, *Angew. Chem. Int. Ed.* **2007**, *46*, 7293.

(51) Anilkumar, G.; Bitterlich, B.; Gelalcha, F. G.; Tse, M. K.; Beller, M. An efficient biomimetic Fe-catalyzed epoxidation of olefins using hydrogen peroxide, *Chem. Commun.* **2007**, 289.

(52) Britovsek, G. J. P.; England, J.; White, A. J. P. Non-heme Iron(II) Complexes Containing Tripodal Tetradentate Nitrogen Ligands and Their Application in Alkane Oxidation Catalysis, *Inorg. Chem.* **2005**, *44*, 8125.

(53) England, J.; Davies, C. R.; Banaru, M.; White, A. J. P.; Britovsek, G. J. P. Catalyst Stability Determines the Catalytic Activity of Non-Heme Iron Catalysts in the Oxidation of Alkanes, *Adv. Synth. Catal.* **2008**, *350*, 883.

(54) England, J.; Gondhia, R.; Bigorra-Lopez, L.; Petersen, A. R.; White, A. J. P.; Britovsek, G. J. P. Towards robust alkane oxidation catalysts: electronic variations in non-heme iron(ii) complexes and their effect in catalytic alkane oxidation, *Dalton Trans.* **2009**, 5319.

(55) Jia, F.; Li, Z. Iron-catalyzed/mediated oxidative transformation of C-H bonds, *Org. Chem. Front.* **2014**, *1*, 194.

(56) Napoly, F.; Kieffer, R.; Jean-Gérard, L.; Goux-Henry, C.; Draye, M.; Andrioletti, B. Fe(TAML)Li/tert-butyl hydroperoxide as a new combination for benzylic C–H oxidation, *Tetrahedron Lett.* **2015**, *56*, 2517.

(57) Wardman, P.; Candeias, L. P. Fenton Chemistry: An Introduction, *Radiat. Res.* **1996**, *145*, 523.

(58) Neyens, E.; Baeyens, J. A review of classic Fenton's peroxidation as an advanced oxidation technique, *J. Haz. Mat.* **2003**, *98*, 33.

(59) Kwan, W. P.; Voelker, B. M. Rates of Hydroxyl Radical Generation and Organic Compound Oxidation in Mineral-Catalyzed Fenton-like Systems, *Environ. Sci. Technol.* **2003**, *37*, 1150.

(60) Dikalov, S. I.; Mason, R. P. Reassignment of organic peroxyl radical adducts, *Free Radical Bio. Med.* **1999**, *27*, 864.

(61) Gan, L.; Huang, S.; Zhang, X.; Zhang, A.; Cheng, B.; Cheng, H.; Li, X.; Shang, G. Fullerenes as a tert-Butylperoxy Radical Trap, Metal Catalyzed Reaction of tert-Butyl Hydroperoxide with Fullerenes, and Formation of the First Fullerene Mixed Peroxides $C_{60}(O)(OOtBu)_4$ and $C_{70}(OOtBu)_{10}$, *J. Am. Chem. Soc.* **2002**, *124*, 13384.

(62) Jira, R. Acetaldehyde from Ethylene—A Retrospective on the Discovery of the Wacker Process, *Angew. Chem. Int. Ed.* **2009**, *48*, 9034.

(63) Smidt, J.; Hafner, W.; Jira, R.; Sedlmeier, J.; Sieber, R.; Rüttinger, R.; Kojer, H. Katalytische Umsetzungen von Olefinen an Platinmetall-Verbindungen Das Consortium-Verfahren zur Herstellung von Acetaldehyd, *Angew. Chem.* **1959**, *71*, 176.

(64) Huff, C. A.; Sanford, M. S. Cascade Catalysis for the Homogeneous Hydrogenation of CO2 to Methanol, *J. Am. Chem. Soc.* **2011**, *133*, 18122.

(65) Li, Y.-J.; Yan, N.; Liu, C.-H.; Yu, Y.; Zhao, Y.-L. Gold/Copper-Co-catalyzed Tandem Reactions of 2-Alkynylanilines: A Synthetic Strategy for the C2-Quaternary Indolin-3-ones, *Organic Letters* **2017**, *19*, 1160.

(66) Fusi, A.; Ugo, R.; Zanderighi, G. M. Homogeneous catalysis by transition metal complexes, *J. Catal.* **1974**, *34*, 175.

(67) Noels, A. F.; Hubert, A. J.; Teyssie, P. Homogeneous catalysis by transition metal complexes. Selective oxidation of cyclohexene by mixed-catalysts containing rhodium(II) complexes, *J. Organomet. Chem.* **1979**, *166*, 79.

(68) Li, S.; Jia, W.; Jiao, N. Copper/Iron-Cocatalyzed Highly Selective Tandem Reactions: Efficient Approaches to Z-γ-Alkylidene Lactones, *Adv. Synth. Catal.* **2009**, *351*, 569.

(69) Nonami, Y.; Baran, J.; Sosnicki, J.; Mayr, H.; Masuyama, A.; Nojima, M. Reaction of Highly Methylated 2-Methylenecycloalkyl Hydroperoxides with $FeSO_4/CuCl_2$. Remarkably Efficient 5-endo-trig or 6-endo-trig Cyclization of the Intermediate Carbon Radicals, *J. Org. Chem.* **1999**, *64*, 4060.

(70) Panda, N.; Jena, A. K. Cu/Fe-catalyzed coupling reactions, *Organic Chem. Curr. Res.* **2015**, *4*, 130.

(71) Huang, H.; Jiang, H.; Chen, K.; Liu, H. Efficient Iron/Copper Cocatalyzed Alkynylation of Aryl Iodides with Terminal Alkynes, *J. Org. Chem.* **2008**, *73*, 9061.

(72) Hamze, A.; Brion, J.-D.; Alami, M. Synthesis of 1,1-Diarylethylenes via Efficient Iron/Copper Co-Catalyzed Coupling of 1-Arylvinyl Halides with Grignard Reagents, *Org. Lett.* **2012**, *14*, 2782.

(73) Rao Volla, C. M.; Vogel, P. Iron/copper-catalyzed C–C cross-coupling of aryl iodides with terminal alkynes, *Tetrahedron Lett.* **2008**, *49*, 5961.

(74) Panda, N.; Jena, A. K.; Mohapatra, S. Ligand-free Fe-Cu Co-catalyzed Cross-coupling of Terminal Alkynes with Aryl Halides, *Chem. Lett.* **2011**, *40*, 956.

(75) Yang, S.; Wu, C.; Zhou, H.; Yang, Y.; Zhao, Y.; Wang, C.; Yang, W.; Xu, J. An Ullmann C-O Coupling Reaction Catalyzed by Magnetic Copper Ferrite Nanoparticles, *Adv. Synth. Catal.* **2013**, *355*, 53.

(76) Liu, X.; Zhang, S. Efficient Iron/Copper-Cocatalyzed O-Arylation of Phenols with Bromoarenes, *Synlett* **2011**, *2011*, 268.

(77) Kovacs, S.; Novak, Z. Oxidoreductive coupling of thiols with aryl halides catalyzed by copper on iron, *Org. Biomol. Chem.* **2011**, *9*, 711.

(78) Wang, Z.; Fu, H.; Jiang, Y.; Zhao, Y. Fe/Cu N,O-arylation, *Synlett* **2008**, 2540.

(79) Guo, D.; Huang, H.; Zhou, Y.; Xu, J.; Jiang, H.; Chen, K.; Liu, H. Ligand-free iron/copper cocatalyzed N-arylations of aryl halides with amines under microwave irradiation, *Green Chem.* **2010**, *12*, 276.

(80) Panda, N.; Jena, A. K.; Mohapatra, S.; Rout, S. R. Copper ferrite nanoparticle-mediated N-arylation of heterocycles: a ligand-free reaction, *Tetrahedron Lett.* **2011**, *52*, 1924.

(81) Reed, S. A.; White, M. C. Catalytic Intermolecular Linear Allylic C−H Amination via Heterobimetallic Catalysis, *J. Am. Chem. Soc.* **2008**, *130*, 3316.

(82) Pankhurst, J. R.; Cadenbach, T.; Betz, D.; Finn, C.; Love, J. B. Towards dipyrrins: oxidation and metalation of acyclic and macrocyclic Schiff-base dipyrromethanes, *Dalton Trans.* **2015**, *44*, 2066.

(83) Givaja, G.; Volpe, M.; Leeland, J. W.; Edwards, M. A.; Young, T. K.; Darby, S. B.; Reid, S. D.; Blake, A. J.; Wilson, C.; Wolowska, J.; McInnes, E. J. L.; Schröder, M.; Love, J. B. Design and Synthesis of Binucleating Macrocyclic Clefts Derived from Schiff-Base Calixpyrroles, *Chem. -Eur. J.* **2007**, *13*, 3707.

(84) Askarizadeh, E.; Devoille, A. M. J.; Boghaei, D. M.; Slawin, A. M. Z.; Love, J. B. Ligand Modifications for Tailoring the Binuclear Microenvironments in Schiff-Base Calixpyrrole Pacman Complexes, *Inorg. Chem.* **2009**, *48*, 7491.

(85) Love, J. B. A macrocyclic approach to transition metal and uranyl Pacman complexes, *Chem. Commun.* **2009**, 3154.

(86) Hastings, C. J.; Pluth, M. D.; Bergman, R. G.; Raymond, K. N. Enzymelike Catalysis of the Nazarov Cyclization by Supramolecular Encapsulation, *J. Am. Chem. Soc.* **2010**, *132*, 6938.

(87) Murase, T.; Horiuchi, S.; Fujita, M. Naphthalene Diels−Alder in a Self-Assembled Molecular Flask, *J. Am. Chem. Soc.* **2010**, *132*, 2866.

(88) Slagt, V. F.; Reek, J. N. H.; Kamer, P. C. J.; van Leeuwen, P. W. N. M. Assembly of Encapsulated Transition Metal Catalysts, *Angew. Chem. Int. Ed.* **2001**, *40*, 4271.

(89) Wang, Z. J.; Clary, K. N.; Bergman, R. G.; Raymond, K. N.; Toste, F. D. A supramolecular approach to combining enzymatic and transition metal catalysis, *Nat. Chem.* **2013**, *5*, 100.

(90) Lewis, E. A.; Tolman, W. B. Reactivity of Dioxygen−Copper Systems, *Chem. Rev.* **2004**, *104*, 1047.

(91) Holland, P. L.; Tolman, W. B. Dioxygen activation by copper sites: relative stability and reactivity of (μ-η^2:η^2-peroxo)- and bis(μ-oxo)dicopper cores, *Coord. Chem. Rev.* **1999**, *190–192*, 855.

(92) Devoille, A. M. J.; Love, J. B. Double-pillared cobalt Pacman complexes: synthesis, structures and oxygen reduction catalysis, *Dalton Trans.* **2012**, *41*, 65.

(93) Askarizadeh, E.; Yaghoob, S. B.; Boghaei, D. M.; Slawin, A. M. Z.; Love, J. B. Tailoring dicobalt Pacman complexes of Schiff-base calixpyrroles towards dioxygen reduction catalysis, *Chem. Commun.* **2010**, *46*, 710.

(94) Givaja, G.; Volpe, M.; Edwards, M. A.; Blake, A. J.; Wilson, C.; Schröder, M.; Love, J. B. Dioxygen Reduction at Dicobalt Complexes of a Schiff Base Calixpyrrole Ligand, *Angew. Chem. Int. Ed.* **2007**, *46*, 584.

(95) Dhar, D.; Yee, G. M.; Spaeth, A. D.; Boyce, D. W.; Zhang, H.; Dereli, B.; Cramer, C. J.; Tolman, W. B. Perturbing the Copper(III)–Hydroxide Unit through Ligand Structural Variation, *J. Am. Chem. Soc.* **2016**, *138*, 356.

(96) Gagnon, N.; Tolman, W. B. $[CuO]^+$ and $[CuOH]^{2+}$ Complexes: Intermediates in Oxidation Catalysis?, *Acc. Chem. Res.* **2015**, *48*, 2126.

(97) Dhar, D.; Tolman, W. B. Hydrogen Atom Abstraction from Hydrocarbons by a Copper(III)-Hydroxide Complex, *J. Am. Chem. Soc.* **2015**, *137*, 1322.

(98) Halvagar, M. R.; Solntsev, P. V.; Lim, H.; Hedman, B.; Hodgson, K. O.; Solomon, E. I.; Cramer, C. J.; Tolman, W. B. Hydroxo-Bridged Dicopper(II,III) and -(III,III) Complexes: Models for Putative Intermediates in Oxidation Catalysis, *J. Am. Chem. Soc.* **2014**, *136*, 7269.

(99) Bordwell, F. G.; Cheng, J.; Ji, G. Z.; Satish, A. V.; Zhang, X. Bond dissociation energies in DMSO related to the gas phase values, *J. Am. Chem. Soc.* **1991**, *113*, 9790.

(100) Snelgrove, D. W.; MacFaul, P. A.; Keith U, I.; Wayner, D. D. M. The role of alkoxyl radicals in Gif (GoAggV) chemistry, *Tetrahedron Lett.* **1996**, *37*, 823.

(101) Katayev, E. A.; Ustynyuk, Y. A.; Lynch, V. M.; Sessler, J. L. Mono-palladium(II) complexes of diamidopyridine-dipyrromethane hybrid macrocycles, *Chem. Commun.* **2006**, 4682.

(102) Reiter, W. A.; Gerges, A.; Lee, S.; Deffo, T.; Clifford, T.; Danby, A.; Bowman-James, K. Accordion porphyrins: Hybrid models for heme and binuclear monooxygenases, *Coord. Chem. Rev.* **1998**, *174*, 343.

(103) Allen, S. E.; Walvoord, R. R.; Padilla-Salinas, R.; Kozlowski, M. C. Aerobic Copper-Catalyzed Organic Reactions, *Chem. Rev.* **2013**, *113*, 6234.

(104) Komiya, N.; Naota, T.; Oda, Y.; Murahashi, S.-I. Aerobic oxidation of alkanes and alkenes in the presence of aldehydes catalyzed by copper salts and copper-crown ether, *J. Mol. Catal. A-Chem.* **1997**, *117*, 21.

(105) Murahashi, S.-I.; Oda, Y.; Naota, T.; Komiya, N. Aerobic oxidations of alkanes and alkenes in the presence of aldehydes catalysed by copper salts, *J. Chem. Soc. Chem. Comm.* **1993**, 139.

(106) Gamez, P.; Arends, I. W. C. E.; Reedijk, J.; Sheldon, R. A. Copper(II)-catalysed aerobic oxidation of primary alcohols to aldehydes, *Chem. Commun.* **2003**, 2414.

(107) Bolm, C.; Schlingloff, G.; Weickhardt, K. Use of molecular oxygen in the Baeyer-Villiger oxidation the influence of metal catalysts, *Tetrahedron Lett.* **1993**, *34*, 3405.

(108) Kushioka, K. Catalytic activity of copper(II)-ethylenediamine complexes in autoxidation of phenols, *J. Org. Chem.* **1983**, *48*, 4948.

(109) Reglier, M.; Jorand, C.; Waegell, B. Binuclear copper complex model of tyrosinase, *J. Chem. Soc. Chem. Comm.* **1990**, 1752.

(110) Halfen, J. A.; Young, V. G.; Tolman, W. B. An Unusual Ligand Oxidation by a (μ-η^2:η^2-Peroxo)dicopper Compound: 1° > 3° C−H Bond Selectivity and a Novel Bis(μ-alkylperoxo)dicopper Intermediate, *Inorg. Chem.* **1998**, *37*, 2102.

(111) Hay, A. S. Process for the preparation of 3, 3', 5, 5'-tetra-substituted diphenoquinone, **1965**, US Patent 3,210,384,

(112) Ken, T.; Yohei, S.; Tetsuya, S.; Katsuomi, T. Selective Oxidation of Phenols to Hydroxybenzaldehydes and Benzoquinones with Dioxygen Catalyzed by Polymer-Supported Copper, *Bull. Chem. Soc. Jpn.* **2002**, *75*, 311.

(113) Yamaguchi, J.; Yamaguchi, A. D.; Itami, K. C-H Bond Functionalization: Emerging Synthetic Tools for Natural Products and Pharmaceuticals, *Angew. Chem. Int. Ed.* **2012**, *51*, 8960.

(114) Faulkner, D. J. Interesting aspects of marine natural products chemistry, *Tetrahedron* **1977**, *33*, 1421.

(115) Devoille, A. M. J.; Richardson, P.; Bill, N. L.; Sessler, J. L.; Love, J. B. Selective Anion Binding by a Cofacial Binuclear Zinc Complex of a Schiff-Base Pyrrole Macrocycle, *Inorg. Chem.* **2011**, *50*, 3116.

(116) Gao, Y.; Guery, J.; Jacoboni, C. $FeCl_3$ behavior in acetonitrile: structures of $[FeCl_2(CH_3CN)_4][FeCl_4]$ and $[AlCl(CH_3CN)_5][FeCl_4]_2.CH_3CN$, *Acta Crystallographica Section C* **1993**, *49*, 147.

(117) İnam, R.; Bilgin, C. Square wave voltammetric determination of methiocarb insecticide based on multiwall carbon nanotube paste electrode, *J. Appl. Electrochem.* **2013**, *43*, 425.

(118) Tang, Y.; Huang, R.; Liu, C.; Yang, S.; Lu, Z.; Luo, S. Electrochemical detection of 4-nitrophenol based on a glassy carbon electrode modified with a reduced graphene oxide/Au nanoparticle composite, *Anal. Methods* **2013**, *5*, 5508.

(119) Lee, A.-C.; Liu, G.; Heng, C.-K.; Tan, S.-N.; Lim, T.-M.; Lin, Y. Sensitive electrochemical detection of horseradish peroxidase at disposable screen-printed carbon electrode, *Electroanalysis* **2008**, *20*, 2040.

(120) Eaton, S. S.; Eaton, G. R.; Chang, C. K. Synthesis and geometry determination of cofacial diporphyrins. EPR spectroscopy of dicopper diporphyrins in frozen solution, *J. Am. Chem. Soc.* **1985**, *107*, 3177.

(121) Eaton, S. S.; More, K. M.; Sawant, B. M.; Eaton, G. R. Use of the EPR half-field transition to determine the interspin distance and the orientation of the interspin vector in systems with two unpaired electrons, *J. Am. Chem. Soc.* **1983**, *105*, 6560.

(122) Stößer, R.; Herrmann, W. Physical and Chemical Response of $FeCl_3/FeCl_4^-$ Spin Probes on the Functionalizing of Ionic Liquids, *J. Phys. Chem. A,* **2013**, *117*, 3960.

(123) Barton, D. H. R. Gif chemistry: The present situation, *Tetrahedron* **1998**, *54*, 5805.

(124) Barton, D. H. R.; Hu, B.; Taylor, D. K.; Wahl, R. U. R. The selective functionalization of saturated hydrocarbons. Part 32. Distinction between the Fe-Fe and Fe-Fe manifolds in Gif chemistry. The importance of carboxylic acids for alkane activation. Evidence for a dimeric iron species involved in Gif-type chemistry, *J. Chem. Soc. Perk. T. 2* **1996**, 1031.

(125) Barton, D. H. R.; Costas Salgueiro, M.; MacKinnon, J. The functionalization of saturated hydrocarbons. Part 39. Further evidence for the role of the iron-carbon bond in Gif chemistry, *Tetrahedron* **1997**, *53*, 7417.

(126) Gozzo, F. Radical and non-radical chemistry of the Fenton-like systems in the presence of organic substrates, *J. Mol. Catal. A-Chem.* **2001**, *171*, 1.

(127) Perkins, M. J. A radical reappraisal of Gif reactions, *Chem. Soc. Rev.* **1996**, *25*, 229.

(128) Minisci, F.; Fontana, F.; Araneo, S.; Recupero, F. New syntheses of mixed peroxides under Gif-Barton oxidation of alkylbenzenes, conjugated alkenes and alkanes; a free-radical mechanism, *J. Chem. Soc. Chem. Comm.* **1994**, 1823.

(129) Minisci, F.; Fontana, F.; Araneo, S.; Recupero, F. New free-radical syntheses under Gif-Barton oxidation conditions, *Tetrahedron Lett.* **1994**, *35*, 3759.

(130) Muchalski, H.; Levonyak, A. J.; Xu, L.; Ingold, K. U.; Porter, N. A. Competition H(D) Kinetic Isotope Effects in the Autoxidation of Hydrocarbons, *J. Am. Chem. Soc.* **2015**, *137*, 94.

(131) Knight, C.; Perkins, M. J. Concerning the mechanism of 'Gif' oxidations of cycloalkanes, *J. Chem. Soc. Chem. Comm.* **1991**, 925.

(132) Weber, M.; Fischer, H. Absolute Rate Constants for the β-Scission and Hydrogen Abstraction Reactions of the tert-Butoxyl Radical and for Several Radical Rearrangements: Evaluating Delayed

Radical Formations by Time-Resolved Electron Spin Resonance, *J. Am. Chem. Soc.* **1999**, *121*, 7381.

(133) MacFaul, P. A.; Ingold, K. U.; Wayner, D. D. M.; Que, L. A Putative Monooxygenase Mimic Which Functions via Well-Disguised Free Radical Chemistry1, *J. Am. Chem. Soc.* **1997**, *119*, 10594.

(134) Arends, I. W. C. E.; Ingold, K. U.; Wayner, D. D. M. A Mechanistic Probe for Oxygen Activation by Metal Complexes and Hydroperoxides and Its Application to Alkane Functionalization by $[Fe^{III}Cl_2$tris(2-pyridinylmethyl)amine$]^+$ BF_4, *J. Am. Chem. Soc.* **1995**, *117*, 4710.

(135) Kochi, J. K. The mechanism of the copper salt catalysed reactions of peroxides, *Tetrahedron* **1962**, *18*, 483.

(136) Groves, J. T.; McClusky, G. A. Aliphatic hydroxylation via oxygen rebound. Oxygen transfer catalyzed by iron, *J. Am. Chem. Soc.* **1976**, *98*, 859.

(137) Itô, R.; Migita, T.; Morikawa, N.; Simamura, O. Influence of substituent groups in the arylation of substituted benzenes by aryl radicals derived from p-substituted N-nitrosoacetanilides, *Tetrahedron* **1965**, *21*, 955.

(138) Avila, D. V.; Ingold, K. U.; Lusztyk, J.; Dolbier, W. R.; Pan, H. Q.; Muir, M. Absolute rate constants for some reactions of perfluoro-n-alkyl radicals in solution, *J. Am. Chem. Soc.* **1994**, *116*, 99.

Table of Contents Synopsis

A dicopper Pacman complex acts as a cooperative catalyst for the oxygenation of benzylic C-H bonds by organic peroxides when activated by ferric chloride. Analytical and solution spectroscopies suggest an interaction between the dinuclear copper unit and the chloride of $FeCl_3$ occurs, and a full kinetic modelling of the reaction reveals a network of oxidation pathways, via the formation of metal-associated radical intermediates.

Table of Contents graphic